J Low Temp Phys (2008) 150: 101–122
DOI 10.1007/s10909-007-9521-8

Cryogenic Boiling and Two-Phase Flow during Pipe Chilldown in Earth and Reduced Gravity

Kun Yuan · Yan Ji · J.N. Chung · Wei Shyy

Received: 2 August 2007 / Accepted: 10 October 2007 / Published online: 1 November 2007

Abstract For many industrial, medical and space technologies, cryogenic fluids play indispensable roles. An integral part of the cryogenic transport processes is the chilldown of the system components during initial applications. In this paper, we report experimental results for a chilldown process that is involved with the unsteady two-phase vapor-liquid flow and boiling heat transfer of the cryogen coupled with the transient heat conduction inside pipe walls. We have provided fundamental understanding on the physics of the two-phase flow and boiling heat transfer during cryogenic quenching through experimental observation, measurement and analysis. Based on the temperature measurement of the tube wall, the terrestrial cryogenic chilldown process is divided into three stages of film boiling, nucleate boiling and single-phase convection that bears a close similarity to the conventional pool boiling process. In earth gravity, cooling rate is non-uniform circumferentially due to a stratified flow pattern that gives rise to more cooling on the bottom wall by liquid filaments. In microgravity, there is no stratified flow and the absence of the gravitational force sends liquid filaments to the central core and replaces them by low thermal conductivity vapor that significantly reduces the heat transfer from the wall. Thus, the chilldown process is axisymmetric, but longer in microgravity.

Keywords Cryogenics · Boiling heat transfer · Two-phase flow · Chilldown · Microgravity

PACS 44.35.+c · 45.55.Dp · 47.55.-t

K. Yuan · Y. Ji · J.N. Chung (✉)
Department of Mechanical and Aerospace Engineering, University of Florida, Gainesville, FL 32611-6300, USA
e-mail: jnchung@ufl.edu

W. Shyy
Department of Aerospace Engineering, University of Michigan at Ann Arbor, Ann Arbor, MI 48109-2140, USA

1 Introduction

Cryogenic fluids are widely used in industrial, aerospace, cryosurgery systems and so on. For example, liquid hydrogen is used in industrial applications such as metal processing, plate glass production, fat and oil hardening, semiconductor manufacturing, and pharmaceutical and chemical manufacturing. In these systems, proper transport, handling and storage of cryogenic fluids are of great importance. However, the chilldown or quenching process which initiates cryogenic fluids transport is complicated, involving unsteady two-phase heat and mass transfer, and has not been fully understood.

1.1 Role of Cryogenics in Space Exploration

The extension of human space exploration from a low earth orbit to a high earth orbit, then to Moon, Mars, and possibly asteroids and moons of other planets is one of NASA's biggest challenges for this new millennium. Integral to this is the effective, affordable, and reliable supply of cryogenic fluids. The efficient and safe utilization of cryogenic fluids in thermal management, power and propulsion, and life support systems of a spacecraft during space missions involves the transport, handling, and storage of these fluids in terrestrial and reduced gravities.

Chilldown process is the inevitable initial stage during cryogenic fluid transport. Due to their low boiling points, boiling and two-phase flows are encountered in most of the cryogenic operations. The complexity of the problem results from the intricate interaction of the fluid dynamics and heat transfer, especially when phase-change (boiling and condensation) is involved. Because of the large stratification in densities between the liquid and vapor phases, the reduced gravity condition in space would strongly change the terrestrial flow patterns and accordingly affect the momentum and energy transport characteristics. Therefore, boiling and two-phase flow behave quite differently when the gravity levels are varied. The uncertainties about the flow pattern, pressure drop and heat transfer characteristics pose a severe design concern. For example, there is considerable disagreement over the chilldown heat fluxes and whether a unique rewetting temperature exists [1, 2]. Different definitions of rewetting temperatures are reported in chilldown researches: Leidenfrost temperature, minimum film boiling temperature, quenching temperature from thermocouple observations and the temperature at which critical heat flux occurs [1]. For similar experimental observations, quiet different explanations were also suggested by different researchers. For example, it was reported that the rewetting velocity increased with increasing inlet flow rate, given the same initial wall temperature [3–5]. Duffey and Porthouse [4] suggested that the flow rate effect resulted from increasing the wet side heat transfer coefficient with higher inlet flow. This improves the rate of axial heat conduction and hence leads to a faster rewetting rate. Thompson [5], however, argued that the inlet flow rate affects precooling on the dry side rather than the heat transfer in the wet side. Additionally, because of the experimental difficulties, in general, there is very little heat transfer data for cryogenic flow boiling in reduced gravity. A representative work is reported by Adham-Khodaparast et al. [6].

The proposed research will focus on addressing specific fundamental and engineering issues related to the microgravity two-phase flow and boiling heat transfer

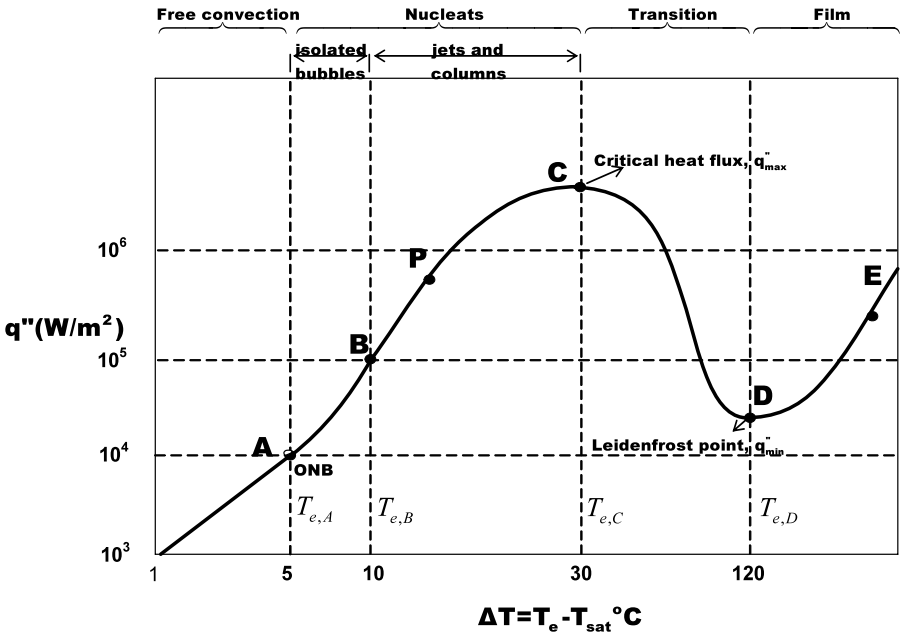

Fig. 1 Typical boiling curve

of cryogenic fluids that require well-designed and meaningful experimentation. In this paper, liquid nitrogen chilldown process is investigated and divided into several stages based on the flow image and temperature data. The outcome of the research will provide fundamental understanding on the transport physics of cryogenic boiling and two-phase flows in a reduced gravity.

2 Background and Literature Review

2.1 Boiling Curve

A boiling curve shows the relationship between the heat flux that the heater supplies to the boiling fluid and the heater surface temperature. According to the typical boiling curve as shown in Fig. 1, a cryogenic chilldown (quenching) process usually starts from point E and then goes towards point D in the film boiling regime as the wall temperature decreases. Point D is called the Leidenfrost point which signifies the minimum heater temperature required for the film boiling. For the film boiling process, the wall is so hot that liquid will vaporize before reaching the heater surface which causes the heater to be always in contact with vapor. When cooling beyond the Leidenfrost point, if a constant heat flux heater were used, then the boiling would shift from film to nucleate boiling (somewhere between points A and B) directly with a substantial decrease in the wall temperature because the transition boiling is an unstable process. If the heater wall temperature can be controlled independently, then the boiling process will proceed from D to C in the transition boiling mode.

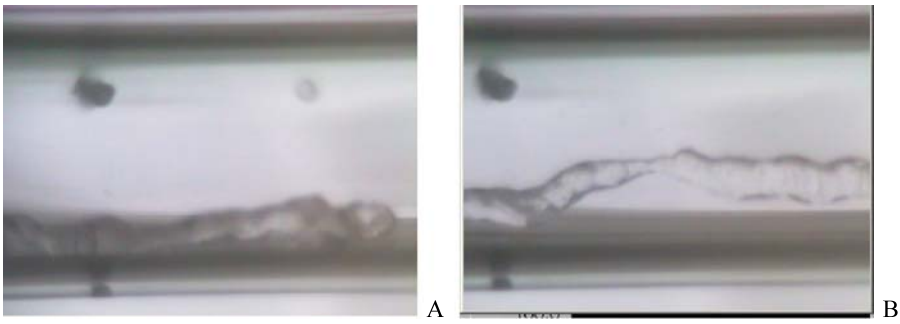

Fig. 2 Gravity effect on flow patterns. **A** Flow pattern in 1-g test. **B** Flow pattern in microgravity test

2.2 The Effects of Gravity

Because of the differences in density and inertia, the two phases in the flow are usually non-uniformly distributed across the pipe under the terrestrial condition. The absence of gravity has important effects on flow patterns, pressure drop and heat transfer. Surface-tension-induced forces and surface phenomena are likely to be much more important in outer space than they are on earth. Actually, all flow-pattern-specific phenomena will be influenced by the gravity level [7]. As an example, in one of our own experiments, for the same mass flow rates, Fig. 2 compares the flow patterns under both terrestrial and microgravity conditions and the difference is significant as the liquid filament is on the bottom and suspended in the middle of the tube for terrestrial and microgravity conditions, respectively.

Momentum and energy transport in two-phase flow and boiling under microgravity is a relatively new field. This is a complex problem for the scientific community to solve. The rewards are rich, however, as new ways to propel future space missions and more intensive space activities have been planned. Currently, there exists a limited quantity of literature, data, and test facilities to even begin to answer these questions. Microgravity cryogenic boiling research was initiated more than fifty years ago, but the progress has been limited. The following summarizes the accomplishments.

2.3 Terrestrial Cryogenic Boiling and Two-Phase Flow

Numerous studies of cryogenic boiling in the one-g environment were conducted in the 1950s and 60s. Brentari et al.'s work [8] is a comprehensive review of the experimental studies and heat transfer correlations. For oxygen, nitrogen, hydrogen and helium, it was found that for pool boiling, the Kutateladze [9] correlation had the greatest reliability for nucleate boiling while the Breen and Westwater [10] correlation was best for film boiling. Maximum nucleate flux data were reasonably well predicted by the Kutateladze correlation. Although these correlations were selected as the best available, neither has particularly good agreement with experimental data. For the case of forced convection boiling, Brentari et al. [8] reported that no correlation was found to be distinctly better. Some simple predictive methods were found to work as well as more complex schemes. In all boiling cases, it was questioned as

to whether or not the predictive correlations include all of the significant variables that influence the boiling process. In particular, it was suggested that more detailed and better controlled experiments are needed and that more attention to surface and geometry effects is required.

Another comprehensive review of cryogenic boiling heat transfer addressing hydrogen, nitrogen and oxygen is given by Seader et al. [11]. It was reported that nucleate pool boiling results cannot be correlated by a single line but cover a range of temperature difference for a given heat flux. The spread is attributed to surface condition and geometry, and orientation. Maximum heat flux can be reduced by about 50% when going from normal-g to near zero-g. Seader et al. [11] reported a fair amount of data for film pool boiling. Film boiling heat flux is reduced considerably at near zero-g conditions. Only a very limited amount of data is available for subcooled or saturated forced convection boiling and few conclusions were drawn. Relatively recent correlations have been published for normal-g saturated flow boiling of cryogens using the Convection, Boiling and Froude numbers as correlating parameters [12–15]. For example, Van Dresar et al. [15] experimentally studied the near-horizontal two-phase flow of nitrogen and hydrogen. Unlike most of the other works which based on turbulent liquid flow, their work focused on laminar liquid flow conditions and the results for low mass and heat flux flow were correlated with Froude number.

2.4 Reduced Gravity Cryogenic Boiling and Two-Phase Flow

In general, there is little heat transfer data for cryogenic flow boiling in reduced gravity. We were able to find just two reports. Adham-Khodaparast et al. [6] have investigated the flow film boiling during quenching of R-113 on a hot flat surface. They reported lower heat transfer rates during microgravity as compared to normal gravity and contributed that to thickening of the vapor layer. The wall superheat and the surface heat flux at the onset of rewetting and maximum heat flux were found to increase with the inlet liquid subcooling, mass flux and gravity level. The effect of gravity was determined to be more important for low flow rates and less relevant for high flow rates. Antar and Collins [16] reported flow visualization and measurements for flow film boiling of liquid nitrogen in tubes on board KC-135 aircraft. They were particularly interested in the vapor/liquid flow pattern and the thermal characteristics. They identified a new vapor/liquid flow pattern that is unique in low gravity. They also observed that a sputtering leading core followed by a liquid filament annular flow pattern. This new flow pattern is composed of a long and connected liquid column that is flowing in the center of the tube and is surround by a thick vapor layer. The vapor annulus that separates the liquid filament from the wall is much thicker than that observed in the terrestrial experiment. They attributed the filamentary flow to the lack of difference in the speed of vapor and liquid phases. On the heat transfer side, they reported that the quench process is delayed in low gravity and the tube wall cooling rate was diminished under microgravity conditions.

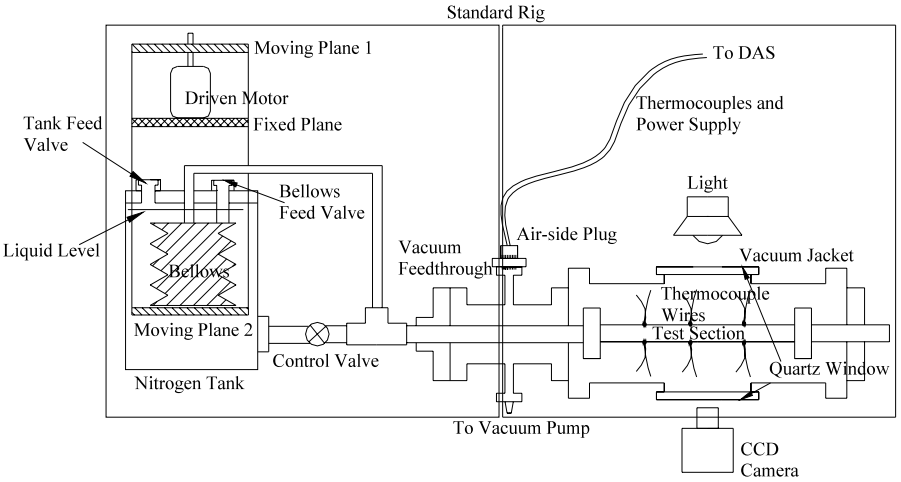

Fig. 3 Schematic of cryogenic boiling and two-phase flow test apparatus

3 Experimental System

To investigate the cryogenic chilldown process, a liquid nitrogen two-phase flow experimental facility has been designed, fabricated and tested under both terrestrial and microgravity conditions. A drop tower is used to provide the microgravity condition.

The experimental system is designed as a once-through flow pass using either gravity or motor-driven bellows as flow generator. Fig. 3 shows the schematic of the experimental system, which locates in two side-by-side aluminum cubicles and is fabricated for both terrestrial and microgravity experiments. The experimental system mainly consists of a nitrogen tank, a motor-driven bellows, test section inlet portion, test section, test section outlet portion, vacuum jacket, vacuum pump, data acquisition system, lighting and video system. A photographic view of the apparatus is shown in Fig. 4. Each component in the system is described separately below.

3.1 Flow Delivery Mechanisms

We have used two different flow delivery systems, one is a gravity-driven flow and the other is a constant flow rate bellows-driven flow. In the gravity-driven system, an insulated reservoir is used to generate the flow. By reviewing the recorded flow images, the mass flux in the gravity flow is estimated to be between 18–23 kg/m^{2}s which provides a liquid entering flow velocity around 3–4 cm/s.

In the bellow-driven system, we followed the traditional method to control cryogenic flow, where the nitrogen flow is generated by a motor-driven stainless steel bellows (Fig. 5). The basic idea is using a constant speed motor to pull a moving plate which is attached to the bottom of a bellows filled with liquid nitrogen. The bellows is submerged in liquid nitrogen inside a nitrogen tank. During the experiment, the state of the flow at the exit of the bellows is saturated liquid. As the bellows being compressed at a constant speed, a constant volumetric flow rate can be achieved,

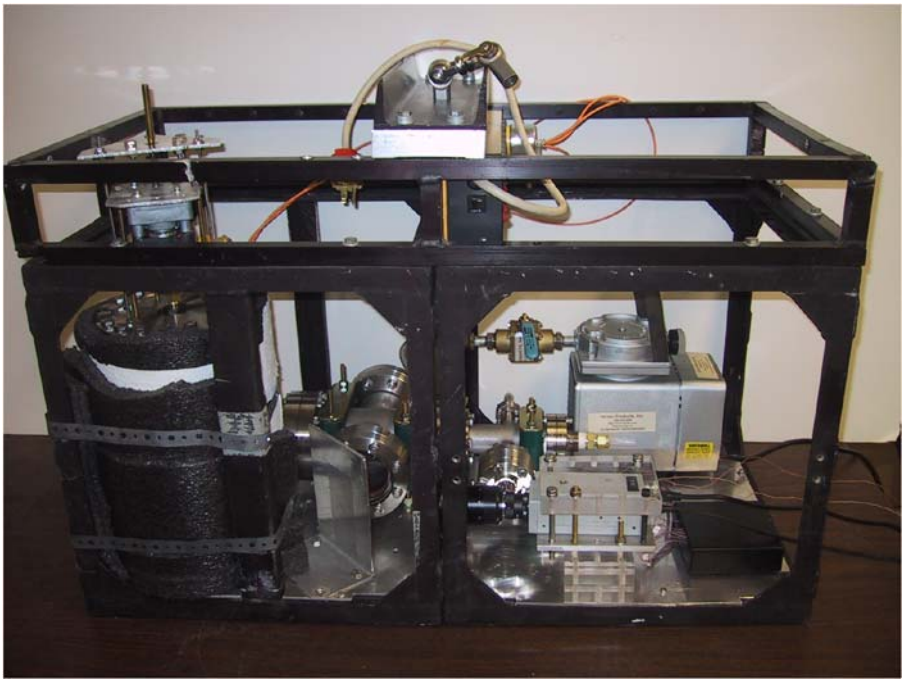

Fig. 4 (Color online) Experimental apparatus located in cubicles

and the corresponding mass flow rate can be calculated. Details of the flow delivery component are given in Yuan et al. [17]. Table 1 shows the three motor speeds used in the experiment and the corresponding mass flux, flow velocity and maximum time of operation. It is noted that the bellows-driven flows are considered lower flow rates while the gravity driven flows are higher flow rates.

3.2 Test Section

The test section is a Pyrex glass tube of 25.4 cm long. The ID and OD of the test section are 11.1 mm and 15.8 mm, respectively. The test section inlet and outlet are stainless steel tubes. At both ends of the test section, stainless steel adaptors and Teflon ferrules are used to connect the test section to the test section inlet and outlet portion.

There are nine drilled holes of approximately 2 mm depth in the test section. The diameter of each hole is 1 mm. A total of 16 type-T thermocouples are placed on the test section, nine are embedded very close to the inner surface through drilled holes at three downstream cross-sections. At each cross-section, three thermocouples are located circumferentially at equal separation distance. The other seven thermocouples are used to measure the outside wall temperatures at two cross-sections, also located circumferentially at equal separation distance. The test section can be rotated along its axis before being fastened at two ends. Figure 6 sketches the test section and the thermocouple locations in one of the tests. Figure 7 is a photograph of the test tube with attached thermocouples.

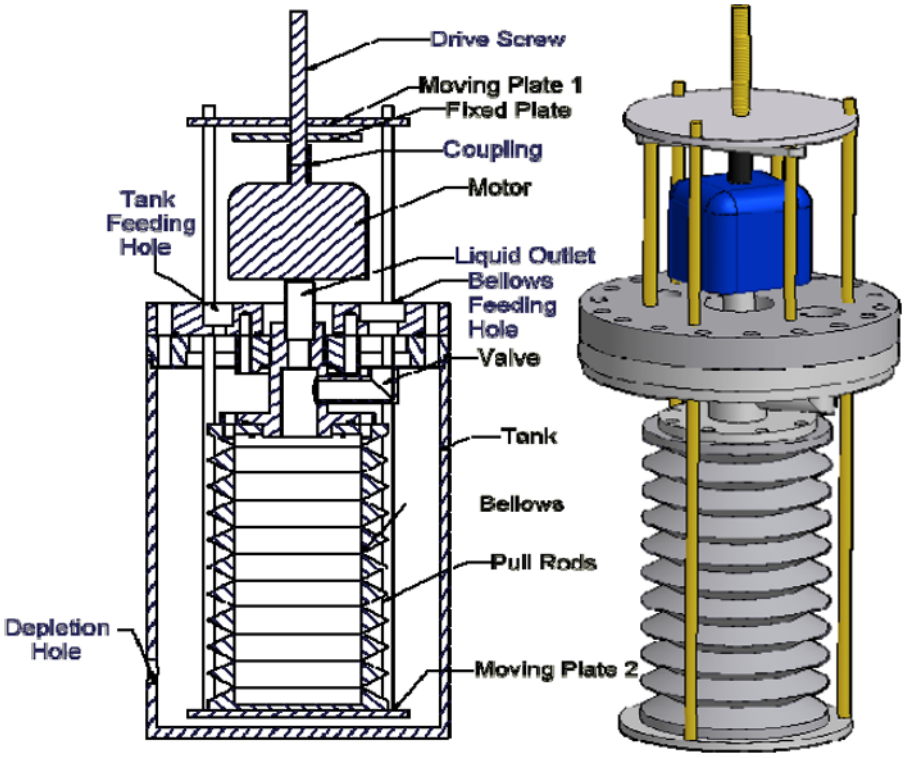

Fig. 5 (Color online) Cryogenic flow driven system

Table 1 Bellows-driven flow delivery system parameters

Motor speed (rpm)	Liquid velocity entering the test section (cm/s)	Mass flux (kg/m^2s)	Approximated test duration limit (minute)
5	0.446	3.606	15
10	0.891	7.205	7.5
15	1.337	10.811	5

The test section inlet, test section and test section outlet are enclosed in a vacuum jacket built from stainless steel vacuum components. Two transparent quartz windows in the vacuum jacket enable the observation and record of the two-phase flow regimes inside the test section. The diameter of each window is 7.62 cm. A ceramic sealed vacuum feed-through flange is used to connect the thermocouple wires from the vacuum side to the air side. The vacuum is maintained by a potable vacuum pump during the experiments. A CCD camera (CV-730 from Motion Analysis Inc.) faces one of the quartz windows to record flow images, while lighting is provided by a fluorescent light at the other widow.

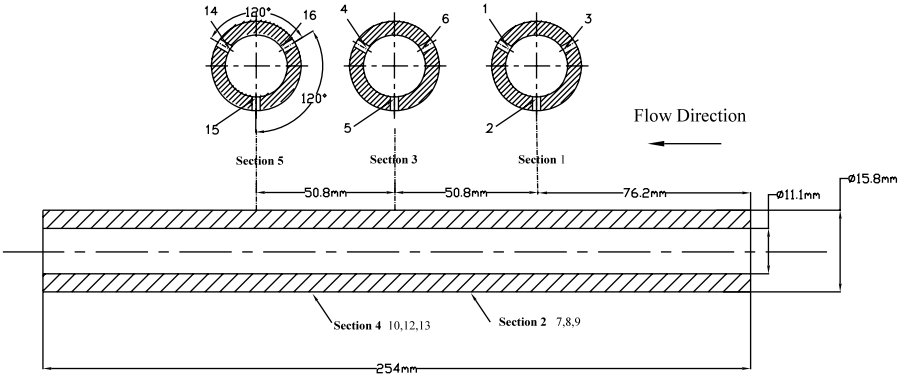

Fig. 6 Test section and thermocouple locations

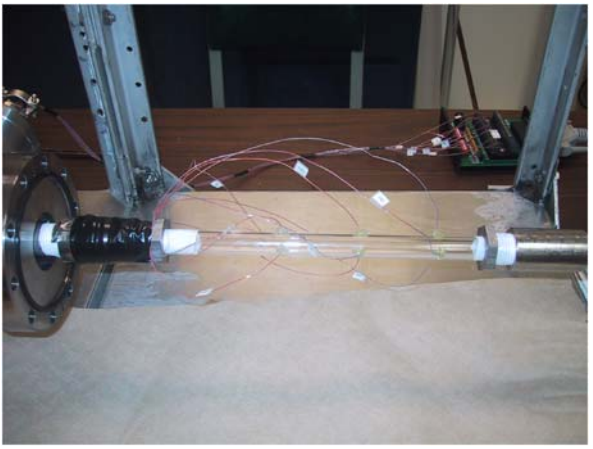

Fig. 7 (Color online) Photograph of cryogenic two-phase flow test apparatus

3.3 Drop Tower Apparatus

The microgravity environment was provided by the University of Florida drop tower. The drop tower is 5-story high and is equipped with an airbag for deceleration. Figure 8 shows the overall drop tower schematic. At the current drop height of 15.25 m, UF's drop tower produces 1.7 seconds of free fall. The experiment is actually located in a drag shield which prevents the experiment from the aerodynamic drag. As a result, the microgravity level is measured between 10^{-5} to 10^{-4}g. Details of the drop tower system and its operation are given in Yuan et al. [17].

3.4 Data Acquisition Component and Experimental Uncertainties

A data acquisition system is built for recording temperatures and flow images during experiments. Type-T thermocouples (Omega) are used for temperature measurement. The thermocouples are wired to a screw terminal board and then connected to a 16-channel thermocouple board (PCI-DAS-TC from Measurement Computing) plugged

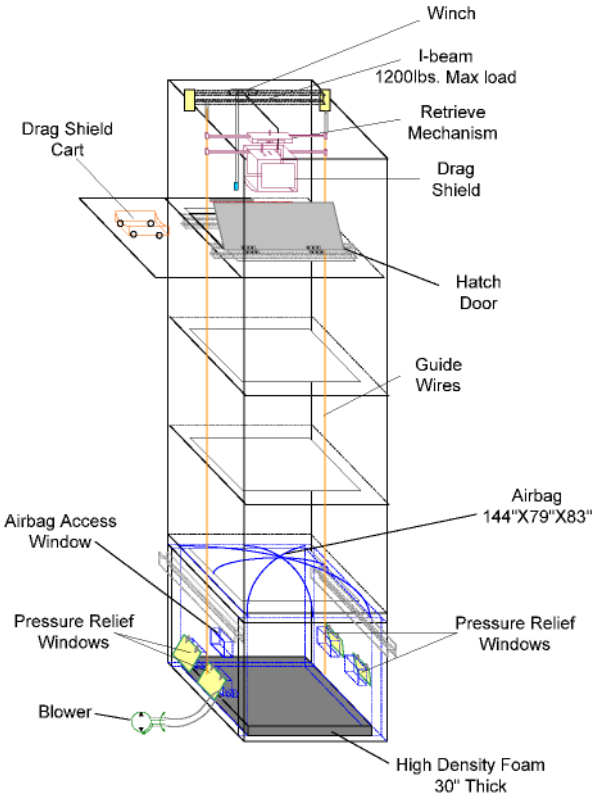

Fig. 8 (Color online) A schematic of the drop tower system

into the PCI slot of a computer. All the thermocouples are tested and calibrated with boiling nitrogen prior to the chilldown experiments. A Labview program is developed to read the temperature measurements to the computer. Video images are monitored and recorded by connecting the CCD camera to a frame grabber board. A commercial software records the flow images and also shows the real-time images on the computer screen.

For the bellows-driven system, the uncertainty of mass flux mainly comes from accuracy of the driven-motor speed, and it is calculated that the relative error for mass flux measurement is 6.88%. The type-T thermocouples used for temperature measurement have the uncertainty of ± 0.5°C declared by the manufacturer. For highly transient process like chilldown the response time of the thermocouples is also important. To get quick response, the tip style of the thermocouples is chosen as exposed and the wire diameter of the thermocouples is used as smaller as possible. With the wire diameter of 0.25 mm the responding time is less than 0.2 second according to the chart given by the manufacturer.

Another uncertainty source of temperature measurement comes from the data acquisition (DAQ) system. The DAQ board for temperature measurement has programmable gain ranges and A/D pacing, and accepts all the thermocouple types. The accuracy of the measurement depends on the gain, the sample rate and the thermocouple type. The uncertainty of type-T thermocouple is ± 0.9°C for worst case from the prod-

uct specification. For current experiment, the gain is set at 400 and the sample rate is about 60 Hz. It is found that the uncertainty for current settings is about ±0.3°C. The relative error for mass flux measurement is ±6.88%.

4 Experimental Results and Discussion

During the "pipe chilldown" experiment, cryogenic transport pipes experience a fast cooling on the walls due to an initially large temperature difference (liquid nitrogen at 77 K and wall at 300 K). The purpose of the chilldown experiment is to provide an overall characterization of the system that includes both flow visualization and heat transfer measurements, and also to offer flow patters and heat transfer characteristics during the pipe chilldown process that takes place in many cryogenic applications in a room temperature environment. The following discussions are classified into two categories: low flow rates (bellows-driven) and high flow rates (gravity driven).

In the beginning of the chilldown experiment, liquid nitrogen enters the Pyrex glass tube that is at the room temperature (25°C). The bulk velocities of the entering liquid flows are estimated in the range of 0.5 to 4 cm/s with both gravity-driven and bellow-driven techniques. With this flow range, the role of gravity is measured by the dimensionless Froude number, Fr which defined as the ratio of flow inertia to gravitational force, $U^2/\mathrm{g}D$, where U is the entering bulk velocity, g is the gravitational acceleration constant and D is the tube diameter. If the Fr number is much larger than unity, then the flow inertia is dominant that renders the gravity insensitive. On the other hand, if the Fr number is much less than unity, then gravity is dominant. The range of the Fr number corresponding to the flow velocities between 0.5 and 4 cm/s is from 1.83×10^{-4} to 1.47×10^{-2}. Since the Fr number is less than unity by two orders of magnitude, it is safe to conclude that gravity plays an important role for both gravity-driven and bellow-driven flows, but the gravity is totally dominant for the bellows-driven case. Because the glass tube is unheated, the tube wall is going through a transient cooling process. In the following, the measured wall temperature history is presented first and then flow visualization pictures are given to provide the correlations between the wall temperature and flow pattern.

4.1 Gravity-Driven Flows—High Flow Rate Case

4.1.1 Boiling Phenomenon during Quenching

Terrestrial Gravity Case For the chilldown process, the temperature histories of the tube walls were measured by the thermocouples at three downstream locations (near inlet, middle and near outlet). The results are given in Fig. 9. Based on the characteristics of the temperature history curves, the chilldown process is generally divided into three stages: (i) Film boiling, (ii) Nucleate boiling and (iii) Single-phase convection.

(i) **Film boiling**. At the beginning of the process, the wall temperature of the test section is near the room temperature, which is much higher than the temperature of the liquid nitrogen and above the Leidenfrost pint, therefore film boiling is taking

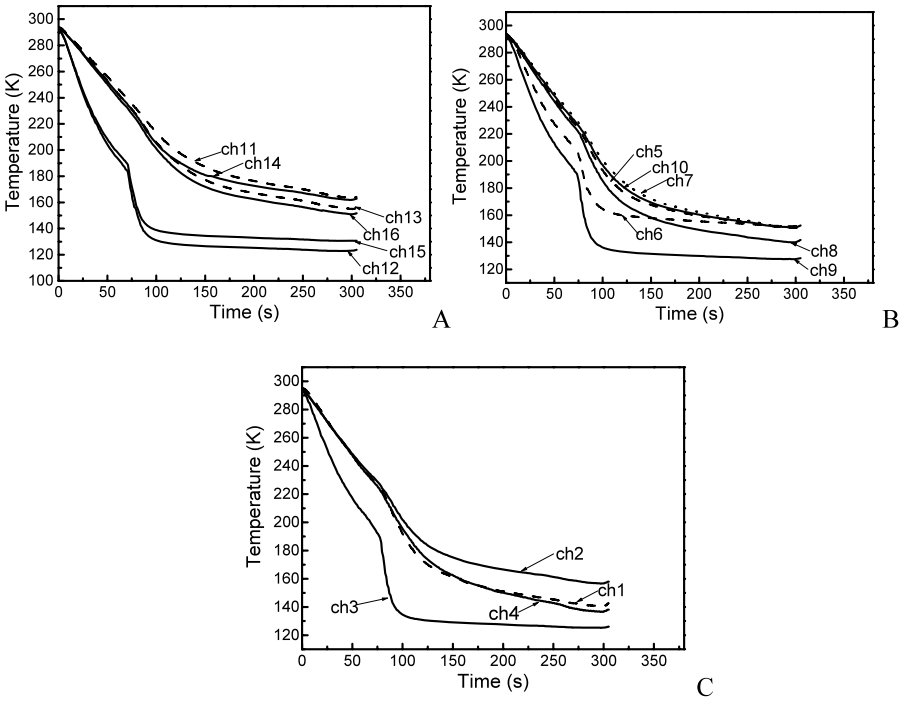

Fig. 9 Temperature profiles at three downstream locations during the chilldown process. **A** Temperature profile of section 1 (near inlet). **B** Temperature profile of section 2 (middle point), **C** Temperature profile of section 3 (near outlet)

place on the tube wall surface. Based on the flow visualization presented in the next section, the initial quenching stage is associated with a hot wall which causes the two-phase flow to take the form of a vapor core with scattered small liquid chunks (Dispersed Flow Film Boiling, DFFB). In general, the temperatures measured by thermocouples that are located in the bottom of the tube (Channels 12, 15, 9, 6 and 3) are lower than those from thermocouples embedded in the upper portion. This is mainly due to the gravity effects that bring liquid fragments cooling to the bottom walls.

(ii) **Nucleate boiling**. A distinctive character of the bottom wall temperature history is the sharp increase in the slope at the wall temperature of about 190 K. This phenomenon is seen at all three downstream locations. The physical explanation is based on the transition of boiling regimes from film boiling to transition boiling and then to nucleate boiling as mentioned earlier and shown in Fig. 1. Even though, the transition boiling regime is very short.

(iii) **Single-phase convection**. Finally when the wall is chilled down enough such that the wall temperature (<140 K, point A in Fig. 1) is too low to support nucleate boiling, the heat transfer switches to single-phase forced convective boiling

(iv) **Chilldown boiling curve.** A 2-D transient conduction model is used to calculate heat transfer data from the transient temperature profiles [17]. In this model, energy balance is performed locally on a control volume of the tube wall at inside wall

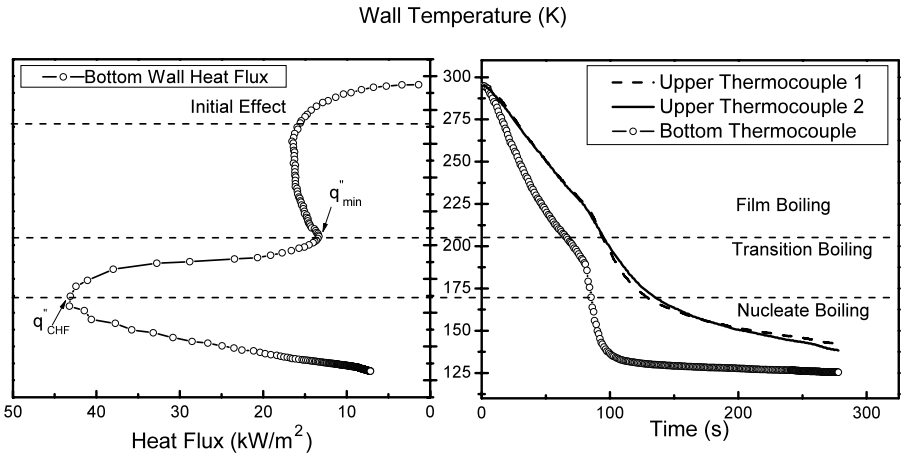

Fig. 10 Estimated heat transfer coefficient

thermocouple location. The change in stored heat in the control volume is equated to the heat transported to the fluid and heat transferred by conduction, minus losses to the environment. The error of this model is evaluated to be in the range of 5–11%.

Based on the temperature data, the heat transfer coefficient history for the bottom wall at section 1 is estimated using the temperature data and plotted in Fig. 10. Left side of Fig. 10 shows the calculated bottom wall heat flux as a function of bottom wall temperature at the outlet cross-section, while the right side represents the corresponding temperature profiles re-plotted from Fig. 9C.

The shape of the heat flux on the bottom of the tube is similar to the boiling curve from steady-state pool boiling experiments. This suggests that the chilldown process may share many common features with the pool boiling process. Following the method to characterize different heat transfer mechanisms in pool boiling experiments, a local maximum or critical heat flux (CHF) q''_{CHF} and a local minimum heat flux q''_{min} are used to divide the chilldown heat transfer into three stages, which are film boiling, transition boiling and nucleate boiling, as shown in Fig. 10 similar to that defined in Fig. 1 for pool boiling.

Initially, the wall temperature is very high and above the Leidenfrost point, so the liquid phase can not contact the tube wall (non-wettable). As a result, liquid nitrogen evaporates intensively when entering the test section; a vapor film blanket will cover the wall surface and separate the liquid from contacting the wall, the two-phase flow is therefore in the film boiling state. As the wall temperature decreases during quenching and drops below the Leidenfrost temperature, the liquid begins to contact the wall; the heat transfer is in the transition boiling regime, which is characterized by an increasing wall heat flux with a decreasing wall superheat that is contrary to the trends in the film boiling region and nucleate boiling region. After passing through the CHF point the heat transfer mechanism then enters the nucleate boiling regime. The calculated bottom wall heat flux as a function of time is shown in Fig. 11. It is obvious that the time of transition boiling is very short as compared with the other two boiling stages.

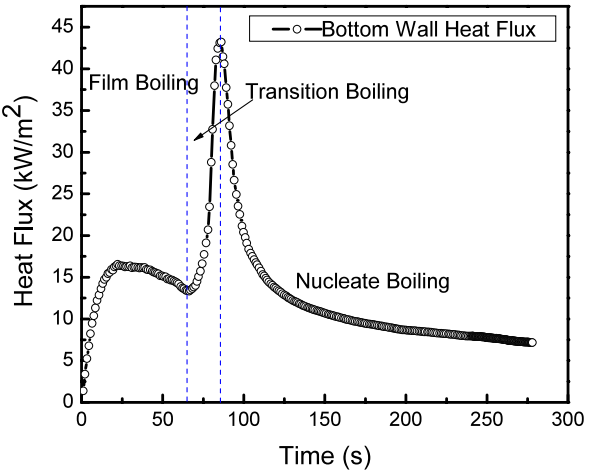

Fig. 11 Bottom wall heat flux at the outlet cross section as a function of time

The similarity between the chilldown boiling curve and the pool boiling curve naturally leads one to compare the chilldown data with pool boiling correlations. The comparison between the two turning points, namely the minimum heat flux and the CHF, is given below. For a steady state film boiling, the correlation developed by Zuber [18] is widely used to predict the minimum heat flux:

$$q''_{\min} = Ch_{lv}\rho_v \left[\frac{\sigma g(\rho_l - \rho_v)}{(\rho_l - \rho_v)^2}\right]^{1/4}. \tag{1}$$

Here, σ is surface tension; g is gravitational acceleration; h_{lv} is the latent heat of vaporization, while C, a constant, was suggested by various researchers as 0.177 [18], 0.13 [19], or 0.09 [20]. The resulting $q''_{\min}$ is then 13.0 kW/m^2, 9.6 kW/m^2, or 6.6 kW/m^2, respectively. In Fig. 11, the $q''_{\min}$ for chilldown is calculated as 13.3 kW/m^2, which is slightly larger than the steady state prediction with $C = 0.177$. Based on the similarity between the CHF condition and the column flooding, Kutateladze [21] derived the following relation for the pool boiling CHF:

$$q''_{\mathrm{CHF}} = 0.131 h_{lv}\rho_v \left[\frac{\sigma g(\rho_l - \rho_v)}{\rho_v^2}\right]^{1/4}. \tag{2}$$

Zuber [18] developed the identical correlation based on the analysis of Taylor and Helmholtz instability. For liquid nitrogen under the atmospheric pressure, (2) gives a CHF value of 160.7 kW/m^2. The chilldown measurement in Fig. 11 is only about 27% of this value. This big discrepancy is believed to come from the following possible sources: (i) Equation (2) was developed for pool boiling over a large horizontal cylinder or a sphere, while the current case is boiling inside a small tube, and (ii) different experimental conditions between the chilldown and the pool boiling processes. In the pool boiling experiment, the heat supplied to the fluid is maintained by a heater, while in chilldown tests it comes from the stored heat in the tube wall. In the film boiling region, the heat flux is generally small, therefore the tube wall can maintain

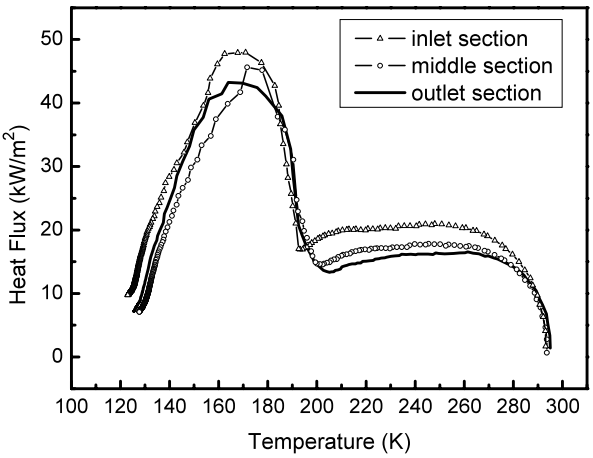

Fig. 12 Bottom wall heat fluxes at different axial locations

a near constant heat flux condition and function like the heater used in the pool boiling tests. However, in the transition boiling region, the stored energy in the tube wall is depleted so quickly that the experimental condition is very different form that of the pool boiling tests. The limited energy stored in the tube wall put a restriction on the value of CHF, which, therefore, is much less than the pool boiling data. Previous work by Bergles and Thompson [22] also quantitatively concluded that the differences between chilldown and steady-state boiling curves can be very large.

For (1) and (2), the minimum heat flux and the CHF, thermal properties of the wall are not factored in the equations. However, as seen from the above, the available heat flux to the flow is closely related to the energy stored in the wall. Therefore, the thermal properties, e.g. thermal conductivity, heat capacity, of the wall are expected to play a role in the chilldown correlations. For example, for a wall with higher thermal conductivity, the energy transferred to the fluid can be more quickly supplied by the walls, and therefore it will result in a higher value of CHF.

Figure 12 shows the estimated heat fluxes in different axial locations of the tube. It is found that both the CHF and the minimum heat flux decrease with increasing axial distance from the inlet. This is also associated with an increase in the rewetting temperature.

In most of the previous quenching experiments, the film boiling heat flux was reported as either a relatively constant value along the axial direction [23, 24] or that it decreases downstreams as the test section is chilled down [22, 25]. In our experiments, however, the local heat flux first increases in a short period then decreases gradually. This is consistent with the transient nature of the experiments. Generally the increasing period is expected to be shorter at higher mass fluxes if the other conditions are kept the same. The mass fluxes in previous investigations were much larger than that in current experiments, and therefore associated with very a short time period of increasing heat fluxes in the film boiling regime. This might be the reason that the increases of the heat flux were not recorded before.

Microgravity Case Because that the gravity-driven flow delivery system could not fit into the limited two-cubicle frame as shown in Fig. 4, therefore we do not have

high-flow rate microgravity results. However, the microgravity drop tower results are provided in the low flow rate section. It is also noted that the gravity effects are dominant for the low flow rate case as mentioned before. But for higher flow rates, we can speculate that the wall temperature history curve in microgravity would be very similar to those of the two upper portion locations (Chaps. 11 and 14 or 13 and 16) where the walls are in contact with vapor phase only. In microgravity, there would be no stratification and a perfect inverted annular flow would prevail, which causes the vapor to cover all the tube wall and leave liquid in the central core area.

4.1.2 Two-Phase Flow Dynamics during Quenching

Terrestrial Condition This phase of the experimentation was intended to provide not only some physical understanding of the two-phase flow characteristics during the chilldown process, but also the performance evaluation for the apparatus which includes both image and data acquisition.

The chilldown process is divided into three stages based on the temperature of the tube wall as discussed above. The initial stage as shown in Fig. 13A is associated with a hot wall which causes the two-phase flow to take the form of a vapor core with scattered small liquid chunks. When the wall becomes slightly cooler, the inverted annular flow is seen as given in Fig. 13B where the liquid is occupying most of the tube with a vapor layer adjacent to the tube wall. For both cases as shown in Figs. 13A and B, it is believed that film boiling is the main mechanism (portion between D and E in Fig. 1). When the wall temperature decreases further, the two-phase flows are experiencing a transition from the film boiling (inverted annular flow) to the stratified flow. Figures. 13C and D show the transition flows for warmer tube walls where liquid chunks are starting to accumulate near the bottom side of the tube wall due to the gravity effects. Finally when the wall is chilled down enough, a stable stratified two phase flow was observed. As shown in Figs. 13E and F, a stable and continuous liquid layer is located on the bottom of the tube and a pure vapor core is flowing on top of the liquid layer. As discussed in the previous section that for the stratified flow here, nucleate boiling (portion between A and B in Fig. 1) is taking place between the liquid layer and the cold bottom wall while the film boiling is the mode between the vapor core and the tube wall. Therefore under the stratified flow, there is a circumferential temperature variation on the tube wall.

As mentioned before, the liquid entering velocity is around 3–4 cm/s but the gravity force is still two orders of magnitude larger than the inertia force as mentioned previously. Therefore, the gravity effect overpowers the flow inertia. This is the reason why we observed the stratified flow when the wall temperature drops below the Leidenfrost point that allows the wall to be wetted by the liquid phase.

Microgravity Case Figure 14 provides a series of two pictures for the chilldown experiment in a microgravity condition. We followed a large chunk of liquid as it traveled downstream. It is seen that basically it is an inverted annular flow where the vapor is filling the tube with liquid chunks in the center. The size of the liquid chunk is decreasing due to vaporization as it flows downstream.

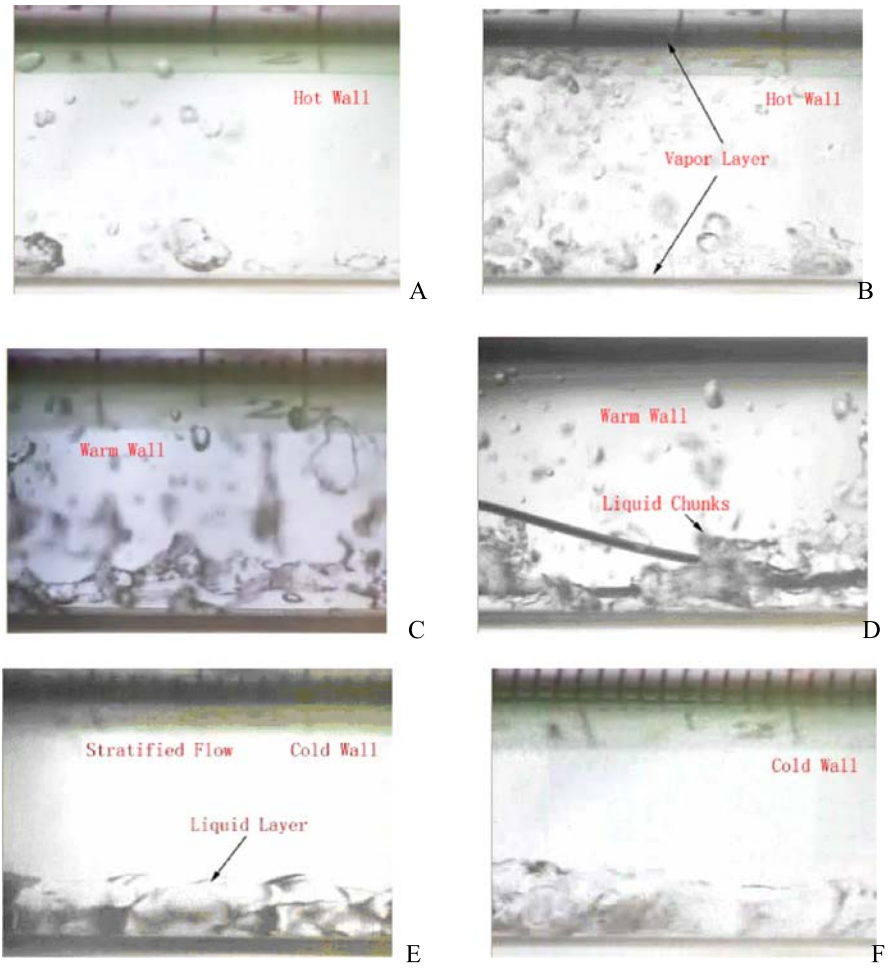

Fig. 13 (Color online) Two-phase flow images under 1-g condition for chilldown process. **A** Initial stage of chilldown-vapor core with scattered liquid chunks. **B** Initial stage—inverted annular flow. **C** Transition stage. **D** Transition stage. **E** Cold wall—stratified flow. **F** Cold wall—stratified flow

4.2 Bellows-Driven Flows—Low Flow Rate Case

4.2.1 Boiling Phenomenon during Quenching

First, for lower flow rates, the gravity dominates more than the flow inertia that makes the cryogenic transport in microgravity to behave differently from that on earth. Also as the flow rate lowers, the heat transfer generally slows down that extends the film boiling period and causes the vapor film to thicken. Especially in microgravity, there is no possibility of a stratified flow and, the heat transfer is generally lower under the microgravity condition due to the replacement of liquid filaments by the vapor film near the bottom walls that makes the chilldown even longer. In this section, the heat

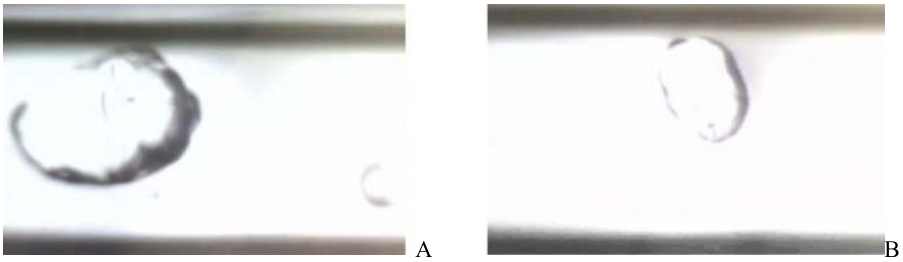

Fig. 14 Photographs of flow pattern in microgravity

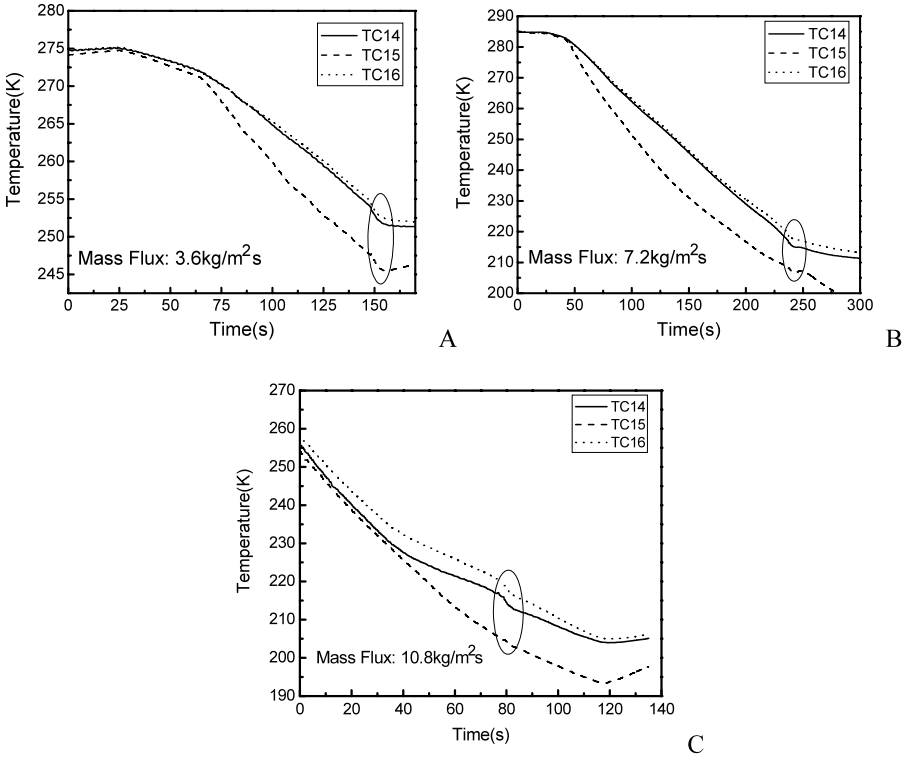

Fig. 15 Temperature profiles with different mass fluxes in microgravity test. **A** Mass flux of 3.6 kg/m^{2}s. **B** Mass flux of 7.2 kg/m^{2}s. **C** Mass flux of 10.8 kg/m^{2}s

transfer and two-phase flow in the film boiling region during chilldown is investigated for both terrestrial and microgravity conditions.

Wall Temperature Profiles To measure more data points during the microgravity period, the wall temperatures are measured only at one cross-section near the inlet. Figure 15 gives the typical temperature profiles with three different mass fluxes.

Based on Fig. 15, the general cooling rate of the tube wall is directly proportional to the mass flow rate of the quenching fluid. The circled temperatures in Fig. 15

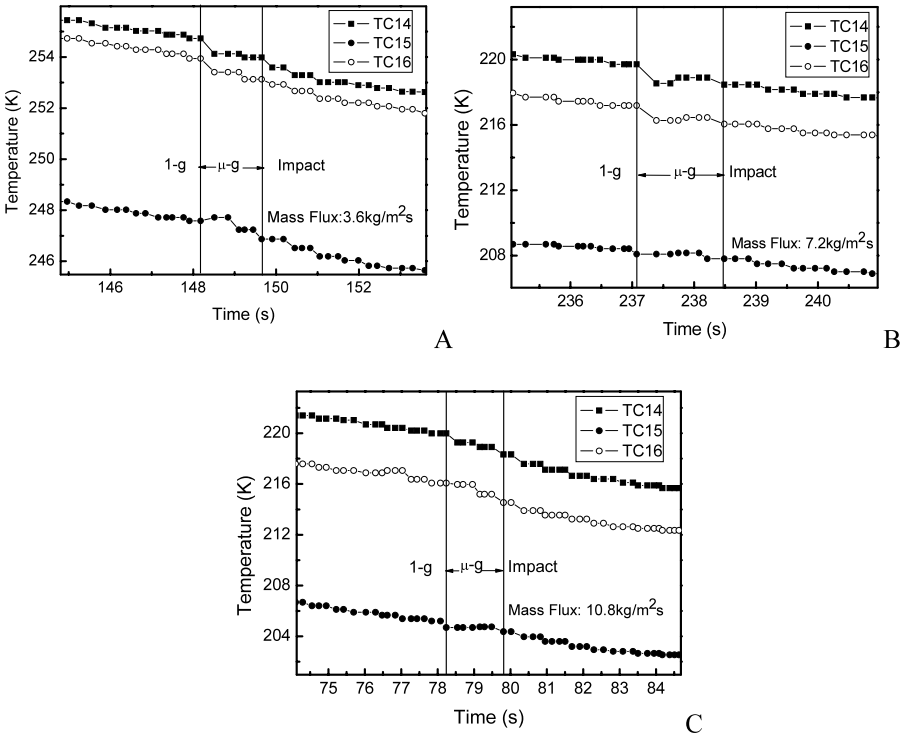

Fig. 16 Wall temperature response to microgravity. **A** Mass flux of 3.6 kg/m^{2}s. **B** Mass flux of 7.2 kg/m^{2}s. **C** Mass flux of 10.8 kg/m^{2}s

approximately indicate the time period of microgravity condition during one drop, which includes the release of the drag shield, microgravity time, impact on the air bag, and deceleration period.

To examine the detail of the wall temperature response to sudden removal of the gravity force, the temperature profiles are zoomed in. Figure 16 illustrates the focused results. It is observed that the temperature decreasing rate at the bottom wall is generally slower during the microgravity period, because the removal of the gravitational force will send liquid filaments to the central core and replace them by low thermal conductivity vapor that significantly reduces the heat transfer from the wall. Since the top wall transfers heat mainly by vapor convection, the gravity field is expected to have negligible effects on the heat transfer at the top wall. For the current transient experimental condition, the best way to represent the data is to calculate the averaged heat flux which is given in the following section.

Wall Heat Flux The gravity effect is shown in Fig. 17, in which the ratio of bottom heat flux before drop and during drop is plotted for different flow rates. The heat flux at the bottom of the tube decreases under microgravity condition and the ratio varies from a minimum of about 0.66 to about 0.90. The result does not show a strong dependence on wall temperature and inlet flow rate. Two runs of the quenching test

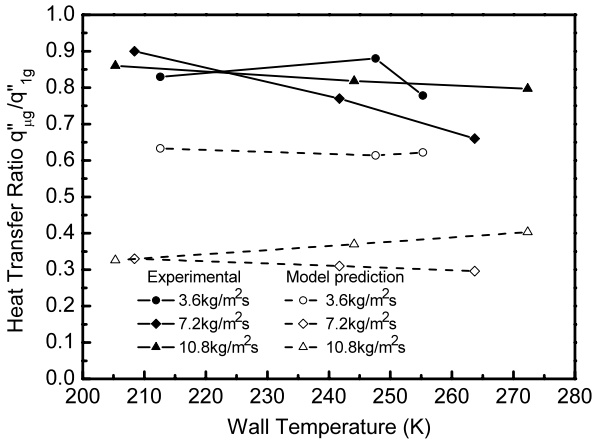

Fig. 17 Ratio of heat flux under microgravity to 1-g condition with different flow rates and comparison with model prediction

performed by Xu [26] reported similar ratio of 0.7 and 0.8, however, in Westbye et al. [23], this ratio was found to be much less and ranged from 0.15 to 0.6.

The bottom wall is subjected to film boiling through the liquid filaments near the wall and the convection to the super heated vapor phase. For the film boiling part, the heat flux and the heat transfer coefficient are proportional to $(a/g)^{1/3}$ as suggested by Merte and Clark [27]. Assuming that the convection is not affected by the microgravity condition, the resulted heat flux ratio is shown in the dash line in Fig. 17; the gravity level in this calculation is 10^{-4}g. The calculation results are much scattered and significantly less than the experimental values. This suggests that under microgravity condition, the effect of convection part may raise the heat flux, and therefore the total effect of the microgravity is less prominent than that in the pool boiling experiments.

4.2.2 Two-Phase Flow Dynamics during Quenching

The flow patterns before (terrestrial gravity) and during drop (microgravity) are compared in Fig. 18 for lower flow rates. The images on the left are taken before the drop, while the microgravity images are on the right.

For all the terrestrial cases, they are all stratified flows. For Fig. 18A the mass flow rate is the lowest, so the liquid flow is in the form of chucks on the bottom wall. For higher flow rates in Figs. 18C, E, and G, the liquid flow on the bottom is in a continuous stream. Different flow behaviors have been recorded during the microgravity period. If the liquid phase before drop is dispersed liquid chunks on the bottom wall, these liquid chunks will enter the central core region still as chunks or stretched ligaments shown in Fig. 18B during the microgravity period. For higher flow rates where continuous liquid filaments are on the bottom in earth gravity, these filaments are lifted up and still maintain their original shapes during the microgravity period (Fig. 18D). In some other cases for even higher flow rates, the larger liquid filaments are broken and dispersed into the central region (Fig. 18F) or has a liquid-vapor core in the center and smaller chunks at both top and bottom (Fig. 18H).

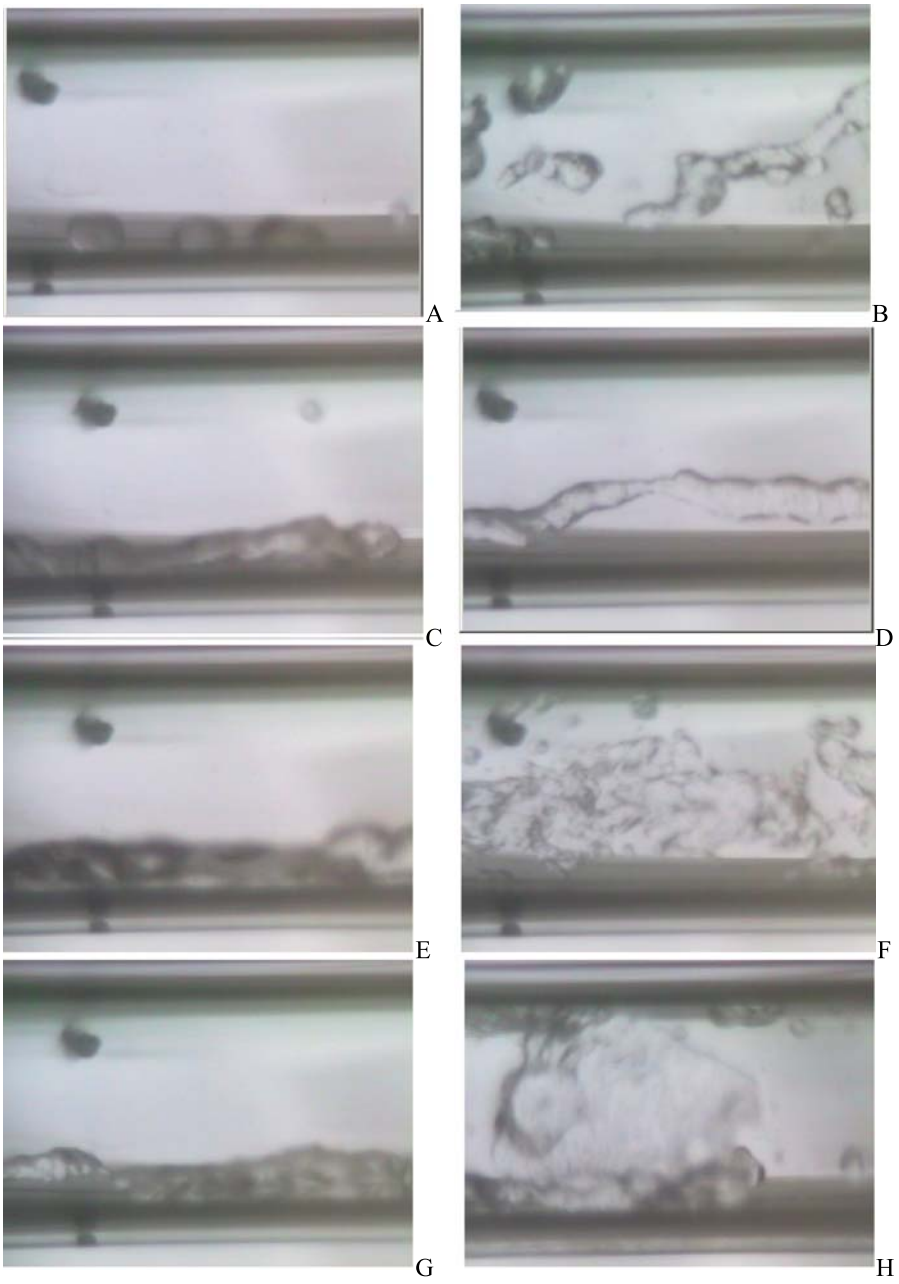

Fig. 18 (Color online) Two-phase flow images under both 1-g and microgravity conditions. **A** 1-g case 1. **B** Microgravity case 1. **C** 1-g case 2. **D** Microgravity case 2. **E** 1-g case 3. **F** Microgravity case 3. **G** 1-g case 4. **H** Microgravity case 4

5 Conclusion

This research is aimed at the fundamental understanding of the cryogenic chilldown phenomena inside a pipe in terrestrial gravity and microgravity. An experimental system was designed, built and calibrated. The microgravity environment was simulated in a 1.7-second drop tower. Flow patterns and wall temperature history during the chilldown were obtained for a range of different flow rates. The wall temperature histories were measured at three downstream locations. Primarily we found that the terrestrial chilldown process is divided into three stages based on the temperature of the tube wall. These stages are film boiling, nucleate boiling and single-phase convection that carries a close similarity to the pool boiling mechanisms. In general, the cooling rate of the tube wall is proportional to the mass flow rate of the quenching flow. In microgravity, there is no stratified flow and because the removal of the gravitational force will send liquid filaments to the central core and replace them by low thermal conductivity vapor that significantly reduces the heat transfer from the wall. Thus, the chilldown process is even longer in microgravity.

Acknowledgements This research was supported by the NASA Hydrogen Research for Spaceport and Space Based Applications at the University of Florida (Grant number NAG3-2930). The support by the Andrew H. Hines, Jr./Progress Energy Endowment Fund is also acknowledged.

References

1. V.K. Dhir, R.B. Duffey, I. Catton, J. Heat Transf. **103**, 293 (1981)
2. B.D.G. Piggott, D.T.C. Porthouse, Nucl. Eng. Des. **32**, 171 (1975)
3. A. Yamanouchi, J. Nucl. Sci. Technol. **5**, 547 (1968)
4. R.B. Duffey, D.T.C. Porthouse, Nucl. Eng. Des. **25**, 379 (1973)
5. T.S. Thompson, Nucl. Eng. Des. **31**, 234 (1974)
6. K. Adham-Khodaparast, J.J. Xu, M. Kawaji, Int. J. Heat Mass Transf. **38**, 2749 (1995)
7. Committee on Microgravity Research, *Microgravity Research in Support of Technologies for the Human Exploration and Development of Space and Planetary Bodies* (National Academy Press, Washington, 2000)
8. E.G. Brentari, P.J. Giarratano, R.V. Smith, *NBS Technical Note*, vol. 317. National Bureau of Standards (1965)
9. S.S. Kutateladze, in *State Sci. and Tech. Pub. of Lit. on Machinery, Moscow* (Atomic Energy Commision Translation 3770) (Tech. Info Service, Oak Ridge, 1952)
10. B.P. Breen, J.W. Westwater, Chem. Eng. Prog. **58**(7), 67 (1962)
11. J.D. Seader, W.S. Miller, L.A. Kalvinskas, Boiling heat transfer for cryogenics. NASA Contractor Report CR-243 (1965)
12. M.M. Shah, Cryogenics **24**, 231 (1984)
13. S.G. Kandlikar, ASME J. Heat Transf. **112**, 219 (1990)
14. K.E. Gungor, R.H.S. Winterton, Chem. Eng. Res. Des. **65**, 148 (1987)
15. N.T. Van Dresar, J.D. Siegwarth, M.M. Hasan, Cryogenics **41**, 805 (2002)
16. B.N. Antar, F.G. Collins, Int. J. Microgravity Sci. Technol. **3**, 118 (1997)
17. K. Yuan, Y. Ji, J.N. Chung, Int. J. Heat Mass Transf. **50**, 4011 (2007)
18. N. Zuber, Ph.D. dissertation, UCLA (1959)
19. N. Zuber, ASME J. Heat Transf. **80**, 711 (1958)
20. P.J. Berenson, ASME J. Heat Transf. **83**, 351 (1961)
21. S.S. Kutateladze, Kotloturbostroenie **3**, 10 (1948)
22. A.E. Bergles, W.G. Thompson, Int. J. Heat Mass Transf. **13** (1970)
23. C.J. Westbye, M. Kawaji, B.N. Antar, AIAA J. Thermophys. Heat Transf. **9**, 302 (1995)
24. S.C. Cheng, H. Ragheb, Int. J. Multiph. Flow **5**, 281 (1979)
25. E.N. Ganić, W.M. Rohsenow, J. Heat Mass Transf. **20**, 855 (1977)
26. J.J. Xu, Ph.D. dissertation, University of Toronto (1998)
27. H. Merte, J.A. Clark, ASME J. Heat Transf. C **86**, 315 (1964)